Robustness of mean field theory for hard sphere models

Giorgio Parisi,[1] Yoav G. Pollack,[2] Itamar Procaccia,[2,3] Corrado Rainone,[2] and Murari Singh[2]

[1]*Dipartimento di Fisica, Sapienza Università di Roma, INFN, Sezione di Roma I,IPFC CNR, Piazzale Aldo Moro 2, I-00185 Roma, Italy*
[2]*Department of Chemical and Biological Physics, Weizmann Institute of Science, Rehovot 76100, Israel*
[3]*Niels Bohr International Academy, Blegdamsvej 17, DK-2100 Copenhagen, Denmark*

In very recent work the mean field theory of the jamming transition in infinite-dimensional hard sphere models was presented. Surprisingly, this theory predicts *quantitatively* the numerically determined characteristics of jamming in two and three dimensions. This is a rare and unusual finding. Here we argue that this agreement is nongeneric: only for hard sphere models does it happen that sufficiently close to the jamming density (at any temperature) the effective interactions are binary, in agreement with mean field theory, justifying the truncation of many-body interactions (which is the exact protocol in infinite dimensions). Any softening of the *bare* hard sphere interactions results in many-body *effective* interactions that are not mean field at any density, making the $d = \infty$ results not applicable.

I. INTRODUCTION

Models of hard sphere fluids and solids have provided useful insights in condensed matter physics and in statistical mechanics for many decades [1,2]. In the last two decades hard spheres played a particularly important role in the investigation of the jamming transition, modeling the solidification of compressed granular matter [3]. The jamming transition is a critical phenomenon, characterized by a number of critical exponents whose values are typically irrational. Careful numerical simulations in two and three dimensions could determine these exponents quite precisely, with three-to five-digit accuracy [4–6]. Direct theoretical calculations in finite dimensions are not available, but a theory in infinite dimensions is available, providing exact predictions as $d \to \infty$ for these critical exponents. It turned out that the predictions at $d \to \infty$ appear to actually agree quantitatively with simulation results in $d = 2$ and 3 [7–9]. In the words of Ref. [10], "One of the most remarkable features of the $d \to \infty$ solution is its agreement with both qualitative and quantitative aspects of jamming observed in numerical simulations. This outcome is especially stunning...." Indeed it is stunning and highly unusual: the critical exponents are usually strongly dependent on dimension, and in many cases turn into mean field values above some critical dimension. For the jamming problem it was found that nontrivial exponents are temperature independent, independent of the density of the jammed packing, and d independent from $d = 2$ to $d \to \infty$.

The aim of this paper is to explain this unusual phenomenon and to argue that it is nongeneric, being fragile to any degree of softening of the hard sphere potential at any finite temperature. The proposed answer is simple: the theory in infinite dimensions is a perturbative approach that enjoys important simplifications by neglecting effective many-body forces that are hard to deal with in finite dimensions [11]. Below we demonstrate that near jamming, this is also the situation for hard spheres in two and three dimensions [12] for any given temperature, but only for hard spheres. Softening the hard sphere potential

at any finite temperature introduces unavoidable many-body effective interactions that mar the correspondence between low and infinite dimensions. We stress here that we are *not* addressing "jamming" with soft potential, a phenomenon that is well defined only at $T = 0$. Rather we are concerned with the relevance of the $d = \infty$ truncation of higher order interactions for any generic finite-temperature glassy calculation.

In Sec. II we discuss the notion of effective forces, which is central to the discussion. The systems that we consider are characterized by bare binary interaction forces. We define the effective forces by considering the time-averaged positions of the particles and ask what are the effective forces that hold these average positions invariant in time. Of course this question can be answered only if the average positions stabilize before diffusion destroys the notion of a stationary average position. This is possible in low-temperature glasses. Then the question is whether these effective forces depend only on the average distance $\bar{\mathbf{r}}_{ij}$ between any pair of particles i and j or do they show dependence on the average positions of other particles. Section III provides the analysis of numerical simulations which highlight the essential difference in answering this question in systems with hard sphere potential and any softened potential. The latter introduces at any finite temperature multibody effective interactions that cannot be neglected, resulting in statistical physics that cannot be captured by mean field infinite dimensional calculations that take into account only binary interactions. Section IV offers a short summary and concluding remarks.

II. EFFECTIVE FORCES

A key concept that underlies the discussion below is that of *effective forces*. These must be distinguished from the *bare forces*. For example in hard spheres the bare forces are zero when there is no contact and infinity upon contact. In a thermal ensemble, particles collide and impart momenta, from which one can compute the effective forces [12]. If the bare

potential is a function of the distance between particles, the effective force can be measured simply as an integral over the force, divided by the total interaction time. Another way to determine the effective forces, which is only appropriate for a glassy system, is to compute the time-averaged positions of the particles $\{\bar{r}_i\}_{i=1}^N$, and ask which effective forces stabilize these averaged positions to make them time independent. The second method [13,14] is more appropriate for experiments in which the momentum transfer or the actual time-dependent bare force are hard to measure. In the simulations below we employ the first method.

To find the effective interactions in hard disks we executed event-driven two-dimensional simulations for systems with fixed area A, a given number of disks $N = 400$ at temperature $T = 1$. The area is square with periodic boundary conditions and all the disks have the same mass m. The disk radii R are slightly polydispersed around a binary 50:50 distribution with mean values and standard deviations of $\langle R_A \rangle = 0.5$, $\sigma_{R_A} = 0.0081$, $\langle R_B \rangle = 0.7$, and $\sigma_{R_B} = 0.0123$. All the hard disk simulations started by determining accurately the area $A_{\text{in}} \equiv L_{\text{in}}^2$ for which the system jams; see Appendix A for details. Then we choose a density ρ for the unjammed systems by expanding the simulation box according to

$$L = L_{\text{in}}(1 + \epsilon). \tag{1}$$

After expanding the system size from the jammed state by the desired ϵ, the simulation is first equilibrated for 2×10^6 collisions and then run for 10^8 collisions. This long run is examined manually to ascertain that it has a section of at least $n_c = 10^7$ collisions in which there are no transitions between meta-basins. Disk positions were measured and averaged-over with the maximal resolution possible (i.e., after each collision). Given a value of ϵ the effective forces f_{ij} were measured by computing the momentum transfer $\Delta_k p(i,j)$ during every kth collision between particles i and j, followed by averaging according to

$$f_{ij} \equiv \frac{\sum_k \Delta_k p(i,j)}{t} \quad \text{for hard spheres}, \tag{2}$$

where t is the total duration of the measurement. One test of the accuracy of the forces f_{ij} is the requirement that they uphold force balance, or

$$f_i = \sum_j f_{ij} = 0. \tag{3}$$

For hard disks this sum rule was obeyed in our numerics to better than 1 part in 10^3 in units of the mean interparticle force. The reader should notice that although we measure f_{ij} by tracking *interactions* between particles i and j it is *not* generally a function of only $\bar{r}_{ij} \equiv \bar{r}_i - \bar{r}_j$. Even in mean field theory one expects that the effective forces between particles i and j will depend on some characteristic of the cages in which they move, in addition to $\bar{r}_{ij}$. In correspondence with the mean field theory of spin glasses [15–18] and liquids [19,20] we can expect a dependence on the mean-square fluctuations in the respective two cages. Defining $K_i \equiv \sqrt{\langle [r_i(t) - \bar{r}_i]^2 \rangle}$ we expect that [21]

$$f_{ij} = g(K_i, K_j, \bar{r}_{ij}) \quad \text{in mean field theory}, \tag{4}$$
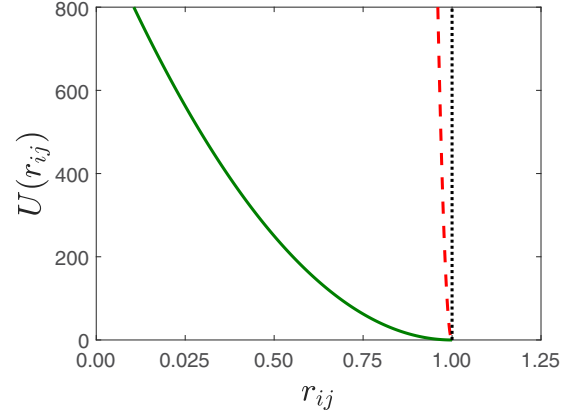
FIG. 1. Comparison between hard and soft potentials used in this paper to underline the fragility of the hard sphere limit. The vertical black line is the hard disk potential and the two others illustrate Eq. (5) with $V_0 = 500\,000$ (red dashed line) and $V_0 = 1000$ (green continuous line).

with g being an *a priori* unknown function. In finite dimensions multiple collisions and the effect of successive collisions cause the effective forces to depend also on the averaged positions of other particles. In other words the effective forces are not in general mean field; see below for more details. We will show, however, that for hard disks sufficiently close to jamming, the effective forces are binary and even independent of K_i and K_j.

To underline the difference between hard spheres and more generic potentials we study here a system of softer disks [3]. Here the system consists of a 50:50 mixture of small (A) and large (B) particles, with diameter ratio of $\lambda_B / \lambda_A = 1.4$. The *bare* interaction potential between particles i and j is given by [22]

$$U(r_{ij}) = \frac{V_0}{2} \left(1 - \frac{r_{ij}}{\lambda_{ij}}\right)^2 \Theta\left(1 - \frac{r_{ij}}{\lambda_{ij}}\right), \tag{5}$$

where r_{ij} is the distance between the centers of mass of particles i and j, $\lambda_{ij} = (\lambda_i + \lambda_j)/2$ is the average diameter, V_0 is the strength of interaction, and Θ is the Heaviside step function. To remain close to the hard sphere limit we choose first a large value of $V_0 = 500\,000$. A second comparison to a softer interaction is achieved with $V_0 = 1000$. The comparison between the hard sphere limit and these two softer potentials is shown in Fig. 1. The units for energy and length are V_0 and λ_A respectively. We integrate the equations of motion for this system using a standard velocity-Verlet algorithm with time step $\Delta t = 0.001$ for $V_0 = 1000$ and $\Delta t = 0.0002$ for $V_0 = 500\,000$. The Nose-Hoover chain thermostat was used to maintain the desired temperature. After expanding the system size from the $(T = 0)$-jammed state by the desired ϵ, we first run the system for time $\tau_1 = 10^5$ (in reduced units). (For more details see Appendix B.) The simulation is then run at constant $T = 10^{-3}$ for a further time of $\tau_2 = 10^6$. All the results pertaining to the soft disks are extracted as described above from a time segment of length $\tau_2/10$. This is again done to avoid transitions between meta-basins. The upshot of this choice is that the average positions were determined using averaging times that are well below the time for which particle

diffusion destroys their meaning. In practice this constrains the values of the expansion ϵ. For values of $\epsilon \geqslant 5.5 \times 10^{-2}$ for hard disks and $\epsilon > 10^{-2}$ for soft disks we could not determine the mean positions of the particles with sufficient accuracy. The average position of the particles are denoted as above as $\{\bar{\boldsymbol{r}}_i\}_{i=1}^N$. In the present case the effective forces are computed from the dynamics according to

$$\boldsymbol{f}_{ij} \equiv -\frac{1}{t}\int_0^t dt' \left(\frac{\partial U}{\partial \boldsymbol{r}_{ij}}\right) \quad \begin{array}{l} \text{for differentiable} \\ \text{bare potential,} \end{array} \quad (6)$$

with t being the time of integration of the dynamics. The sum rule (3) was well obeyed for the soft disks to better than 1 part in 10^6 (in units of the mean interparticle force). Again the main question below will be whether these effective forces are mean field as in Eq. (4), or whether they exhibit many-body interactions.

III. ANALYSIS OF NUMERICAL RESULTS

The analysis is easiest in the case of hard disks with which we begin. In this case we find that near jamming, the effective forces trivialize to binary interactions. To show this we follow two steps: (i) finding for each configuration a function of $\bar{\boldsymbol{r}}_{ij}$ that fits best the effective forces $\boldsymbol{f}_{ij}$; then (ii) measuring the deviations of the data from this best function. The point is that when the effective forces $\boldsymbol{f}_{ij}$ are purely two-body forces they should be a function of $\bar{\boldsymbol{r}}_{ij}$ with a scatter that is only allowed by the accuracy of the measurement, which is extremely high as can be tested by the agreement with Eq. (3). On the other hand when the effective forces include many-body corrections the data should scatter around the best function, with the degree of scatter proportional to the relative significance of the many-body forces.

For hard disks the only energy is T and the only typical scales are h_{ij}, the average gaps between particles [23] $h_{ij} \equiv |\bar{r}_{ij} - R_i - R_j|$, one can expect that if the effective forces were exactly binary then [12]

$$f_{ij} = T/h_{ij}, \quad \text{for hard disks.} \quad (7)$$

In Fig. 2 upper panel we show typical data for f_{ij} as a function of h_{ij} for $\epsilon = 10^{-3}$. We see that the data do not form a function. Next we calculated standard deviation $\sigma_h(\epsilon)$ around the compensated data $f_{ij} \times h_{ij}/T$. This quantity was averaged over different initial configurations for each expansion ϵ. The lower panel of Fig. 2 shows σ_h for different values of ϵ in a log-log plot. The red error bars in this figure stem from the standard deviation between different configurations. The blue error bars represent the accuracy in determining the interparticle forces from Eq. (3). The deviation from purely binary interactions decreases upon approaching jamming:

$$\langle\sigma_h(\epsilon)\rangle \sim \epsilon^\zeta, \quad \zeta \approx 0.15 \pm 0.04. \quad (8)$$

It remains to be seen whether this critical exponent can be derived from known exponents of the jamming criticality or is this a new exponent for the problem at hand.

In the case of soft disks, we have more length scales λ_{ij} to deal with, and guessing the form of a putative limiting effective interaction becomes less obvious. In addition we need now to consider the three different interactions AA, AB, BB. Naive fitting choices like polynomial and rational fits proved not
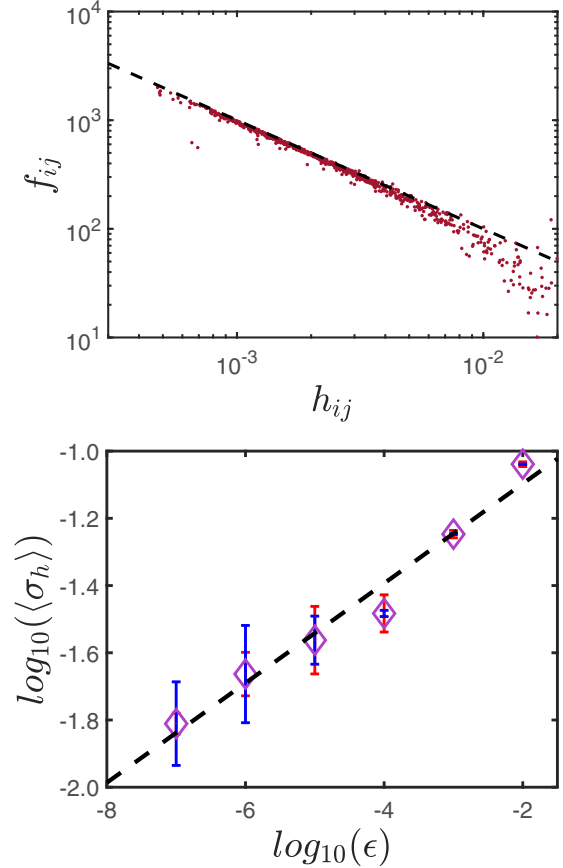
FIG. 2. Upper: Raw data of f_{ij} vs h_{ij} at $\epsilon = 10^{-3}$. The two-body force law [Eq. (7)] is represented by the dashed line. Note that the scatter is not due to inaccuracy as can be tested by the high precision with which Eq. (3) is obeyed. Lower: The standard deviation from the two-body force law for hard disks as a function of the distance from jamming. The dashed line presents the power-law fit of Eq. (8).

to be accurate enough for our purpose (as detailed below). This called for a somewhat more complicated procedure as explained next.

To determine whether in a given system the force law conforms with mean field expectation in Eq. (4) we need first to determine the cage fluctuations K_i. The probability distribution function of K_i was measured for soft spheres using some 77–92 configurations (depending on ϵ). Selecting only pairs of particles with very close values $K_i \approx K_j$ from the peak of this distribution, we used a Padé approximant (of order 1 in the numerator and order 2 in the denominator) to fit the forces f_{ij} as functions of $h_{ij} \equiv \bar{r}_{ij} - \lambda_{ij}$. The function obtained is denoted as $g_1(h_{ij})$. Second, we normalized f_{ij} by this function. Doing this, one discovers that the Padé approximant is not always sufficient, in the sense that f_{ij}/g_1 still retains a clear functional form deviating from unity, see top panel of Fig. 3. We therefore fitted to the normalized forces f_{ij}/g_1 a polynomial of degree 4. The new fit is denoted as $g_2(h_{ij}) \equiv f_{ij}/g_1$. Next we considered, as seen in Fig. 3, the function $f_{ij}/g_1 - g_2$ and determined the standard deviation σ_s of the data scatter around zero. Finally we averaged σ_s among the three interactions, for each expansion parameter ϵ [24].
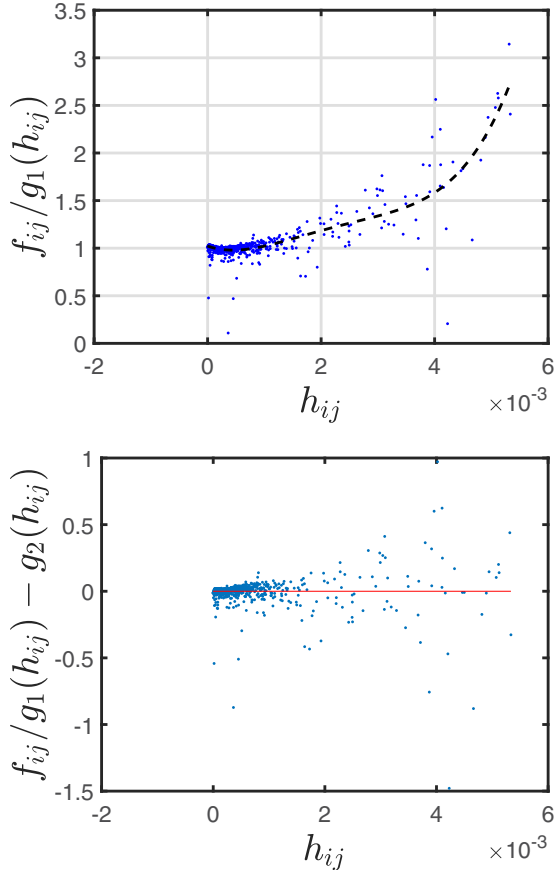
FIG. 3. Procedure followed to determine the deviations from mean field binary force laws in the case of soft spheres with $V_0 = 500\,000$ and $\epsilon = 10^{-4}$. Upper: The first step after normalizing by the Padé approximant. Black dashed line indicates the $g_2(h_{ij})$ fit. Lower: The second step resulting in a scatter around zero. Note that for softer spheres with $V_0 = 1000$ the first step with a Padé approximation is sufficient in many instances.

FIG. 4. Standard deviation from the mean field binary force law for soft spheres as a function of the distance from jamming. Upper: $V_0 = 500\,000$. Lower: $V_0 = 1000$.

many-body forces would provide an accurate theory for any property of finite-temperature glasses made of soft spheres.

Figure 4 shows this $\langle \sigma_s \rangle$ vs ϵ in a log-log plot. For both values of V_0 the difference between the behavior of the hard and soft disks is glaring. In the latter case the importance of the many-body interactions is quite independent of ϵ. In hindsight this is not surprising: even when almost touching, two soft colliding spheres i and j which are in the range of interaction of other soft spheres k, ℓ, etc., should feel their influence; the momentum transferred by the i, j interaction is not determined only by their bare forces, but also by the pull and push of adjacent other disks. In colloquial terms "when push comes to shove it's important who your neighbors are."

It is interesting to notice that in absolute values the degree of non-mean-field many-body contributions increases when the range of interaction increases (the spheres get softer). The above stated intuition is the obvious reason for that. But also one should note that the constant value of many-body contributions for the softer spheres is of the same order as the maximal value of the same contribution for the hard spheres. There is really very little effect of the density on the relative importance of higher-order forces in the case of softer potentials. One *cannot* expect that a truncation of the

IV. CONCLUDING REMARKS

In summary, it was demonstrated that the hard sphere limit is fragile to softening in the sense that non-mean-field interactions remain important at any finite temperature and any density. The conclusion is that it is not likely that mean field calculations in infinite dimensions would provide accurate predictions for the statistical mechanics in finite dimensions for generic bare potentials. This conclusion of course does not detract from the relevance of mean field analytic calculation in indicating the qualitative features of interesting statistical-mechanical problems, including jamming. Further analysis of the emergent many-body interactions in generic cases and their role in the statistical mechanics of thermal glasses will be discussed in future work.

the Simons Fellowship under the auspices of the Niels Bohr International Academy.

APPENDIX A: HARD DISK SIMULATIONS

To create jammed configurations of hard disks we follow the following steps:

(1) Create systems of harmonic disks at a packing fraction $\phi = 0.86$.

(2) Implement the FIRE minimization algorithm [25] coupled to a Berendsen barostat to bring the pressure to 10^{-6}–10^{-7}, depending on the system size.

(3) Use 128-bit numerics from here: impose increments of expansive strain that are proportional to the current pressure, and follow each of these increments by a minimization using the FIRE algorithm (without the barostat, i.e., at constant volume). Repeat until the pressure approaches 10^{-10} or below.

(4) Find the maximal overlap $-h_{ij}$ between any two particles, and expand L precisely to eliminate this maximal overlap.

Having determined the system volume as close to the jammed state as possible, we expand the system size from the jammed state by the desired ϵ, cf. Eq. (1). (Note that the value of L_{in} fluctuated from realization to realization in our finite-size samples). Then the simulation is first equilibrated for 2×10^6 collisions and then run for $n_c = 10^8$ collisions more. As described in Appendix C, for each simulation only a section of $n_c/10$ collisions is used for computing the average positions. This is in order to avoid transitions between meta-basins.

For each value of ϵ the deviation of the force law from the two-body putative interaction was averaged over 20–32 configurations, each taken from a different simulation starting from a different initial condition.

APPENDIX B: HARMONIC DISK SIMULATIONS

We use the velocity-Verlet algorithm with time steps $\Delta t = 0.001, 0.0002$ for $V_0 = 1000, 500\,000$ respectively to integrate the equation of motion. The Nosé-Hoover chain thermostat was used to maintain the desired temperature.

1. Setup of jammed configurations

To create the jammed configurations, we follow the protocol as described in Refs. [3,22]. Starting with a random configuration in a square box at a temperature $T = 0.01$ and low packing fraction of $\phi = 0.65$ the system is allowed to equilibrate. Subsequently the system is quenched to a low temperature $T = 10^{-12}$, at a rate of $\dot{T} = 10^{-4}$. Finally the energy is minimized (using the conjugate-gradient technique).

After reaching the local minimum at initial low packing fraction ϕ_i, we apply the "energy minimization at fixed packing fraction" algorithm [3,22] to obtain the nearest static packing with infinitesimal particle overlaps. The system is compressed or decompressed, followed by conjugate-gradient energy minimization at each step. Compression is chosen when the total energy is zero after minimization while decompression is performed when the total energy is nonzero even after energy minimization, due to overlapping particles. This procedure is terminated when the total potential energy per particle satisfies $U/N < 10^{-16}$ at which point we consider the configuration as
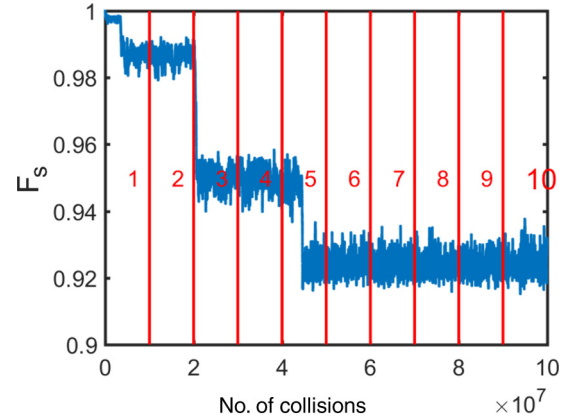
FIG. 5. Self-intermediate scattering function measured for a simulation of hard disks at $\epsilon = 10^{-3}$. Two transitions between meta-basins are clearly evident as sharp drops. The simulation is divided into 10 temporal sections (delimited by red lines and numbered in the figure) in order to choose a section where no such transitions occur.

jammed. Note that the two methods described for hard and soft disks appear different but for all practical purposes are in fact equivalent and could be interchanged.

2. Procedure

As described in Appendix C, for each simulation only a section of $\Delta\tau = \tau_2/10$ is used for computing the average positions. The aim is to avoid transitions between meta-basins. For each value of ϵ, data were taken from 77–92 configurations each taken from a different simulation starting from a different initial condition.

APPENDIX C: TESTING CHANGES IN META-BASINS

To get reliable average positions, we must guarantee that there are no transitions to different meta-basins during measurements. This is achieved by considering three different time-correlation functions: (i) the self-intermediate scattering function, (ii) the mean-square displacement, and (iii) the maximal distance traveled by any single particle. The time correlations are measured every 1000 collisions in the hard disk simulations and at each time step in the harmonic disk simulation. For hard disks, the values of these correlation
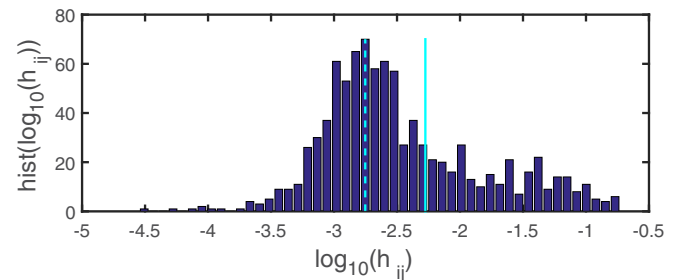
FIG. 6. Histogram of $\log_{10}(h_{ij})$ for a hard disk configuration at expansion $\epsilon = 10^{-3}$. Dashed cyan line indicates the most frequent bin h_{ij}^{freq}. The analysis employs effective forces $\boldsymbol{f}_{ij}$ for which $h_{ij} \leqslant 3h_{ij}^{\mathrm{freq}}$ (solid cyan line).
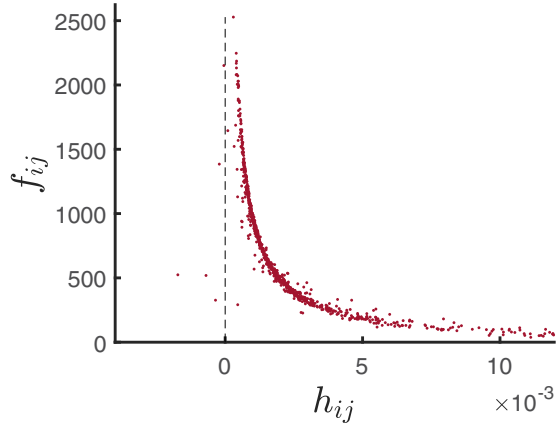
FIG. 7. Effective forces in the hard sphere case with $\epsilon = 10^{-3}$. The data are shown only for small h_{ij} to provide higher resolution around the rare events with negative h_{ij}. The few negative values of h_{ij} are real, stemming from dynamics in which the difference in *average* positions is indeed negative.

functions mostly fluctuate around a constant value (apart from some initial decay and/or growth) with infrequent sharp drops or jumps (see Fig. 5). Such a sharp drop or jump in one of these correlation functions indicates a transition between meta-basins. We divide the simulation into 10 temporal sections (with equal number of collisions and time steps), and for each simulation we analyze a single section in which such transitions were *not* observed. All the average positions are computed within such transition-free sections. This is a stricter criterion than the one used in Ref. [13]. Such sharp drops are observed mostly for the larger expansions $\epsilon \geqslant 10^{-4}$. For smaller expansions the simulation time is too short for transitions to occur. For the soft harmonic disks, the values of the correlation functions can also change smoothly and we choose simulation sections where these values fluctuate around constant values without observable decay or growth. Finally we check that the neighbor list is unchanged in the time intervals for which we compute the average positions.
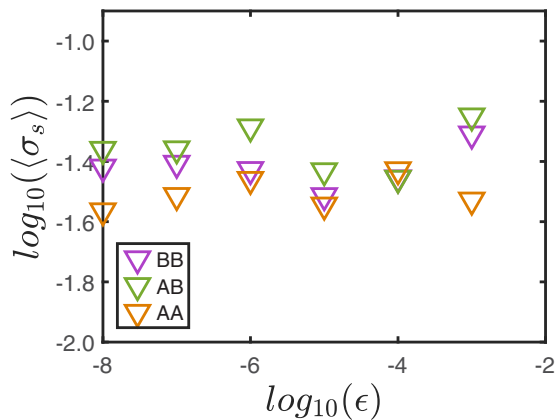
FIG. 8. Standard deviation from the mean field binary force law for soft spheres as a function of the distance from jamming. Here $V_0 = 1000$. Here we used the scalar definition of the distance between pairs and particles and we show the results for each type of interaction (AA, BB, and AB) separately for extra care.
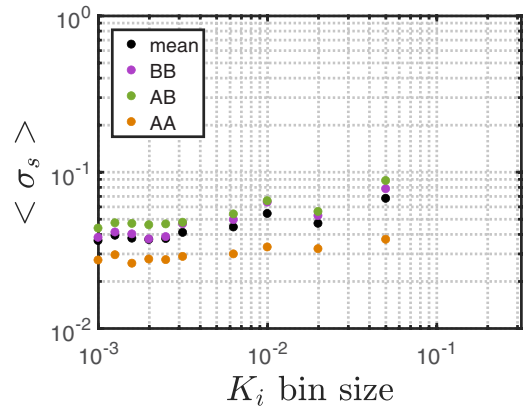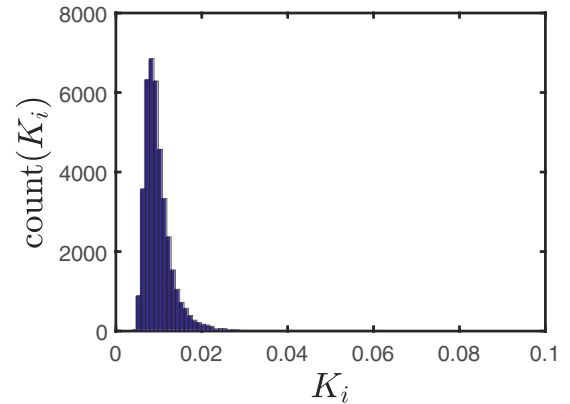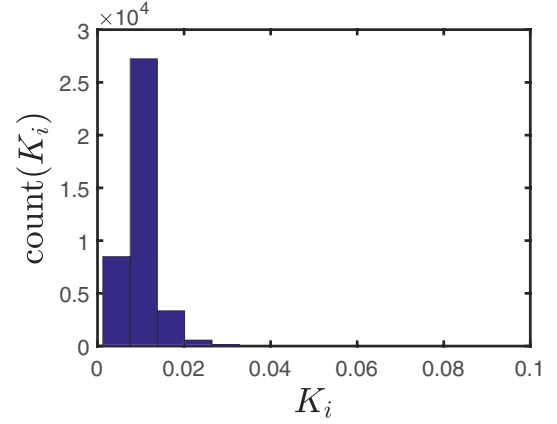
FIG. 9. Upper: The histogram of values of K_i with coarse bins. Middle: The same histogram with finer bins. Lower: The standard deviation around a binary force law as a function of the bin size.

APPENDIX D: CLEANING DATA FROM INFREQUENT COLLISIONS

Hard disks. Configurations of hard disks involve "rattlers" that collide only infrequently compared to typical disks. This introduces errors in the effective force measurements. To clean the data from such outliers we identify the range of h_{ij} that can be trusted. To this aim we plot a histogram of $\log_{10}(h_{ij})$ and bin it into 50 bins, cf. Fig. 6. The value of h_{ij} in the bin with the highest weight is denoted as h_{ij}^{freq}. We then include only effective forces $\boldsymbol{f}_{ij}$ for which $h_{ij} \leqslant 3 \times h_{ij}^{\text{freq}}$.

Harmonic disks. In the case of harmonic disks the "gaps" h_{ij} can be negative, and the cleaning of the data is a bit more

tricky. Instead of using the gap $h_{ij} = r_{ij} - \sigma_i - \sigma_j$, we used $\tilde{h}_{ij} = r_{ij} - r_{ij}^{\min}$ where $r_{ij}^{\min}$ is the minimal r_{ij} of the relevant interaction. We then followed the same procedure as for the hard disks: We plotted a histogram (50 bins) of $\log_{10}(\tilde{h}_{ij})$, found the largest bin $\tilde{h}_{ij}^{\text{freq}}$, and considered effective forces associated with $\tilde{h}_{ij} \leqslant 3 \times \tilde{h}_{ij}^{\text{freq}}$.

Besides cleaning the data from pairs having very large values of h_{ij}, one should also consider for both soft and hard disks some rare configurations that include particle pairs with extremely small and negative values of h_{ij} that deviate strongly from the typical behavior, exhibiting abnormally small forces f_{ij}. These abnormally small f_{ij} were not considered in the analysis. This rare phenomenon disappears when the definition of h_{ij} is changed in favor of a scalar average, and see Appendix E below. At any rate these rare events do not change the general conclusions of the study, as is shown explicitly in Appendix E. To get an impression of the data before the cleanup of negative h_{ij} we present in Fig. 7 some of the effective forces computed for the hard disk case as a function of h_{ij}. It is visually clear that the problematic points are rare.

APPENDIX E: ANALYSIS WITH SCALAR AVERAGING OF DISTANCES r_{ij}

Instead of using the definition of h_{ij} in which $\bar{r}_{ij} \equiv |\frac{1}{\tau} \int_0^\tau dt\, \boldsymbol{r}_{ij}(t)|$ which is computed as a vector average, one could employ a scalar definition of the mean distance between particles,

$$\tilde{h}_{ij} = \tilde{r}_{ij} - R_i - R_j, \quad \tilde{r}_{ij} \equiv \frac{1}{\tau} \int_0^\tau dt\, r_{ij}(t). \quad \text{(E1)}$$

For the case of soft spheres we checked carefully whether this definition may lead to a different conclusion. The answer is negative. As an example we show in Fig. 8 the computed contribution of many-body interactions as a function of ϵ. The overall order of magnitude of the standard deviation reduces compared to the vector definition of the distances, but still there is no indication of approaching the binary limit when $\epsilon \to 0$.

APPENDIX F: RULING OUT MEAN FIELD EFFECTIVE FORCES IN SOFT SPHERES

To determine whether in a given system the force-law conforms with mean field expectations we need to determine the cage fluctuations K_i. The probability distribution function of K_i was measured for soft spheres using some 77–92 configurations (depending on ϵ). Next, we selected pairs of particles from a bin of K_i value with decreasing width of the bin. If Eq. (4) pertains, we should expect that reducing the bin size and plotting the effective forces as a function of h_{ij} must result in reducing the scatter around a functional behavior. In Fig. 9 we show that this is not the case. The data shown pertain to particle pairs whose $K_i \approx K_j$ up to the bin width, selected from the bin with the highest weight. In the upper panel we show the histogram of K_i with large bins, and in the middle panel with finer bins. Finally, in the lower panel we show that the contribution of nonbinary interaction does not reduce when the bins of the histogram get finer and finer. The conclusion is that the mean field expectation of Eq. (4) is untenable in the case of harmonic spheres.

[1] J. Hansen and I. McDonald, in *Theory of Simple Liquids*, 3rd ed., edited by J.-P. Hansen and I. R. McDonald (Academic, New York, 2006).

[2] D. Rapaport, *The Art of Molecular Dynamics Simulation* (Cambridge University, New York, 1997).

[3] C. S. O'Hern, L. E. Silbert, A. J. Liu, and S. R. Nagel, Phys. Rev. E **68**, 011306 (2003).

[4] L. E. Silbert, D. Ertas, G. S. Grest, T. C. Halsey, and D. Levine, Phys. Rev. E **65**, 031304 (2002).

[5] C. S. O'Hern, S. A. Langer, A. J. Liu, and S. R. Nagel, Phys. Rev. Lett. **88**, 075507 (2002).

[6] L. Berthier, D. Coslovich, A. Ninarello, and M. Ozawa, Phys. Rev. Lett. **116**, 238002 (2016).

[7] P. Charbonneau, J. Kurchan, G. Parisi, P. Urbani, and F. Zamponi, Nat. Commun. **5**, 3725 (2014).

[8] P. Charbonneau, E. I. Corwin, G. Parisi, and F. Zamponi, Phys. Rev. Lett. **114**, 125504 (2015).

[9] L. Berthier, H. Jacquin, and F. Zamponi, Phys. Rev. E **84**, 051103 (2011).

[10] P. Charbonneau, J. Kurchan, G. Parisi, P. Urbani, and F. Zamponi, Annu. Rev. Condens. Matter Phys. **8**, 265 (2017).

[11] G. Parisi and F. Zamponi, J. Stat. Mech.: Theory Exp. (2006) P03017.

[12] C. Brito and M. Wyart, Europhys. Lett. **76**, 149 (2006).

[13] O. Gendelman, E. Lerner, Y. G. Pollack, I. Procaccia, C. Rainone, and B. Riechers, Phys. Rev. E **94**, 051001 (2016).

[14] O. Gendelman, Y. G. Pollack, and I. Procaccia, Phys. Rev. E **93**, 060601 (2016).

[15] T. Plefka, J. Phys. A **15**, 1971 (1982).

[16] A. Georges and J. Yedidia, J. Phys. A **24**, 2173 (1991).

[17] A. Altieri, S. Franz, and G. Parisi, J. Stat. Mech. (2016) 093301.

[18] A. Altieri, Phys. Rev. E **97**, 012103 (2018).

[19] H. L. Frisch and J. K. Percus, Phys. Rev. E **60**, 2942 (1999).

[20] G. Parisi and F. Slanina, Phys. Rev. E **62**, 6554 (2000).

[21] In principle one can also consider a dependence on a tensorial quantity $K_i^{\alpha\beta} \equiv \sqrt{[r_i^\alpha(t) - \bar{r}_i^\alpha][r_i^\beta(t) - \bar{r}_i^\beta]}$.

[22] C. F. Schreck, C. S. O'Hern, and L. E. Silbert, Phys. Rev. E **84**, 011305 (2011).

[23] See in Appendix E another, scalar definition of the average gap and its consequences.

[24] Note that in the case of soft spheres we computed the standard deviation from all the samples together, whereas in the hard spheres we averaged over individual configurations. Doing the same in the present work introduces no difference.

[25] E. Bitzek, P. Koskinen, F. Gähler, M. Moseler, and P. Gumbsch, Phys. Rev. Lett. **97**, 170201 (2006).